Mechanisms of the negative shortwave cloud feedback in mid to high latitudes

Article

Published Version

It is advisable to refer to the publisher's version if you intend to cite from the work. See Guidance on citing.

www.reading.ac.uk/centaur

CentAUR

Central Archive at the University of Reading

Reading's research outputs online

Mechanisms of the Negative Shortwave Cloud Feedback in Middle to High Latitudes

PAULO CEPPI AND DENNIS L. HARTMANN

Department of Atmospheric Sciences, University of Washington, Seattle, Washington

MARK J. WEBB

Met Office Hadley Centre, Exeter, United Kingdom

(Manuscript received 5 May 2015, in final form 5 October 2015)

ABSTRACT

Increases in cloud optical depth and liquid water path (LWP) are robust features of global warming model simulations in high latitudes, yielding a negative shortwave cloud feedback, but the mechanisms are still uncertain. Here the importance of microphysical processes for the negative optical depth feedback is assessed by perturbing temperature in the microphysics schemes of two aquaplanet models, both of which have separate prognostic equations for liquid water and ice. It is found that most of the LWP increase with warming is caused by a suppression of ice microphysical processes in mixed-phase clouds, resulting in reduced conversion efficiencies of liquid water to ice and precipitation. Perturbing the temperature-dependent phase partitioning of convective condensate also yields a small LWP increase. Together, the perturbations in large-scale microphysics and convective condensate partitioning explain more than two-thirds of the LWP response relative to a reference case with increased SSTs, and capture all of the vertical structure of the liquid water response. In support of these findings, a very robust positive relationship between monthly mean LWP and temperature in CMIP5 models and observations is shown to exist in mixed-phase cloud regions only. In models, the historical LWP sensitivity to temperature is a good predictor of the forced global warming response poleward of about 45°, although models appear to overestimate the LWP response to warming compared to observations. The results indicate that in climate models, the suppression of ice-phase microphysical processes that deplete cloud liquid water is a key driver of the LWP increase with warming and of the associated negative shortwave cloud feedback.

1. Introduction

Despite continuing model improvement efforts, the cloud feedback remains the largest source of uncertainty in climate sensitivity estimates in global warming experiments (Soden et al. 2008; Boucher et al. 2013; Vial et al. 2013). Uncertainty in the cloud feedback is tied to the difficulty of representing complex, small-scale cloud processes in global climate models. For this reason, accurately portraying the cloud response to warming constitutes a major challenge in the development of future generations of climate models.

Most of the uncertainty in the cloud feedback is associated with the shortwave (SW) component (Soden and Vecchi 2011; Vial et al. 2013). Despite the large uncertainty, one of the few robust aspects of the SW cloud feedback predicted by climate models is a negative feedback occurring in the middle to high latitudes. Unlike the positive subtropical SW cloud feedback predicted by most models, generally associated with a cloud amount decrease, the negative high-latitude feedback is mainly related to an optical thickening of the clouds, resulting in brighter and more reflective clouds (Zelinka et al. 2012; McCoy et al. 2014b; Gordon and Klein 2014).

In liquid and mixed-phase clouds, the primary control on cloud optical depth is the vertically integrated cloud liquid water content, or liquid water path (LWP), which has been shown to be linearly related to cloud optical

Corresponding author address: Paulo Ceppi, Department of Atmospheric Sciences, University of Washington, Box 351640, Seattle, WA 98195.
E-mail: ceppi@atmos.washington.edu

depth in observations (Stephens 1978). The ice water path (IWP) also contributes to the cloud optical depth, but its effect on shortwave radiation is typically smaller due to the larger size of ice crystals compared to liquid droplets (e.g., McCoy et al. 2014a) and because the ice content is typically smaller than the liquid water content. Extratropical LWP increases have been shown to be a robust response to global warming in climate model experiments (Senior and Mitchell 1993; Colman et al. 2001; Tsushima et al. 2006; Kodama et al. 2014; Gordon and Klein 2014) and are therefore likely the main driver of the negative optical depth feedback. Understanding the mechanisms of the negative SW cloud feedback in the middle to high latitudes therefore requires explaining the associated LWP increases.

Various mechanisms have been proposed to explain the predicted LWP increase with warming in the middle to high latitudes. On the one hand, it is natural to expect that liquid water should increase at the expense of ice in mixed-phase clouds as the climate warms (Tsushima et al. 2006; Zelinka et al. 2012; McCoy et al. 2014b; Gordon and Klein 2014). On the other hand, an LWP increase could also result from an increase in the temperature derivative of the moist adiabat with warming, causing enhanced condensation in updrafts (Betts and Harshvardhan 1987; Tselioudis et al. 1992; Gordon and Klein 2014). To further complicate the picture, changes in the hydrological cycle (Held and Soden 2006) and in atmospheric circulation (Barnes and Polvani 2013) may also impact the cloud liquid water content. The possible relevance, and relative importance, of these various processes is currently not well understood.

In this paper, we demonstrate that most of the cloud liquid water increase in the middle to high latitudes in global warming experiments results from a decrease in the efficiency of the processes depleting cloud water. This is due to the suppression of ice-phase microphysical processes with warming, including not only the conversion of liquid water to ice (e.g., through the Wegener–Bergeron–Findeisen process) but also the conversion of cloud condensate to precipitation. The importance of these processes is shown by perturbing temperature in the cloud microphysics schemes of two state-of-the-art climate models, which are run in aquaplanet configuration. The temperature-dependent phase partitioning of detrained condensate from convection is also shown to contribute to the global warming response, although the effect is more modest. Finally, we show that LWP is very robustly linked to temperature in mixed-phase regions in both models and observations, providing further support to the conclusions drawn from our aquaplanet model experiments. The strong observed relationship between LWP and temperature may provide a basis to constrain the negative optical depth feedback in climate models.

We begin by presenting the changes in SW radiation, LWP, and IWP predicted by CMIP5 models in the RCP8.5 twenty-first-century scenario in section 2. We then describe the models and the experimental setup used in this study in section 3, and present our model results in section 4. Evidence for a temperature–LWP relationship in models and observations is provided in section 5. We discuss and summarize our findings in section 6.

2. Cloud–radiative response to global warming

a. Shortwave cloud feedbacks in CMIP5

The multimodel mean SW cloud feedback in the RCP8.5 experiment is presented in Fig. 1a. In both hemispheres, the response features a meridional dipole, with a positive SW cloud feedback in the subtropics and lower midlatitudes ($\sim$10°–45°) and a negative feedback poleward of about 50°. The dipolar structure is reasonably robust, since more than 75% of the models agree on the sign of the feedback on either lobe of the dipole, particularly in the Southern Hemisphere. [Note that the SW cloud feedback shown in Fig. 1a includes rapid adjustments and aerosol forcing (Sherwood et al. 2015); accounting for these effects would affect the magnitude of the cloud feedback but would be unlikely to change the overall meridional structure.]

The main focus of this paper will be on the negative SW cloud feedback at middle to high latitudes, which is associated with large increases in gridbox-mean liquid water path (Fig. 1b). The LWP increase poleward of $\sim$45° is a remarkably robust feature of the RCP8.5 simulations. The mean LWP response is substantial, amounting to an increase by roughly 10% K^{-1} relative to the historical multimodel mean value around 60°. The gridbox-mean ice water path response is smaller and consists of a poleward shift of cloud ice around the midlatitudes. Because there is no compensating large decrease in IWP, total cloud water (liquid + ice) also increases in the middle to high latitudes (not shown).

As discussed in the introduction, the cloud liquid water increase with warming is thought to be the main driver of the negative SW cloud feedback in the high latitudes, by causing an optical thickening and brightening of the clouds (Tsushima et al. 2006; Zelinka et al. 2013; Gordon and Klein 2014; McCoy et al. 2014b). To understand the causes of the negative high-latitude feedback, it is therefore necessary to explain the mechanisms for the LWP increase.

b. Hypotheses for the negative extratropical cloud feedback

Several hypotheses have been proposed in the literature to explain the negative extratropical cloud feedback. We list them below and briefly discuss some open questions associated with them.

1) Phase changes in mixed-phase clouds: In the middle and high latitudes, clouds are commonly mixed-phase (Warren et al. 1988) since supercooled liquid water can exist at temperatures above −38°C. Upon warming, we expect an increase in liquid water at the expense of ice in regions where mixed-phase clouds exist (Senior and Mitchell 1993; Tsushima et al. 2006; Choi et al. 2014). The transition to more liquid clouds may also yield an increase in total condensed water (liquid + ice) because liquid water droplets precipitate less efficiently than ice crystals (e.g., Senior and Mitchell 1993; Klein et al. 2009). The magnitude of the phase change effect in models and observations is still unclear, however, and is likely to depend on microphysical processes whose representation in climate models is difficult and uncertain.

2) Increases in adiabatic cloud water content: As temperature increases, the amount of water condensed in saturated updrafts also increases, assuming the rising air parcels are cooled moist-adiabatically (Somerville and Remer 1984; Betts and Harshvardhan 1987; Tselioudis et al. 1992; Gordon and Klein 2014). It has been suggested that the cloud liquid water increases at middle to high latitudes may reflect an increase in adiabatic cloud water content with warming, which theory predicts to increase more rapidly at lower temperatures (Betts and Harshvardhan 1987; Gordon and Klein 2014). However, changes in other processes that deplete cloud liquid water may also play an important role, such as phase changes to ice, conversion to precipitation, or mixing of the updrafts with the environment (Tselioudis et al. 1992, 1998).

3) Poleward jet shifts: The dynamical response to global warming features a robust poleward shift of the jet streams and storm tracks, particularly in the Southern Hemisphere (Barnes and Polvani 2013). Several studies have proposed that storm track shifts may be associated with shifts in cloudiness, producing a dipole-like radiative anomaly (Bender et al. 2012; Grise et al. 2013; Boucher et al. 2013). However, more recent work has shown that the relationship between jet shifts and cloud–radiative properties is highly model dependent (Grise and Polvani 2014; Ceppi and Hartmann 2015), and the dynamically induced cloud response is both different in structure and much smaller in magnitude than the global
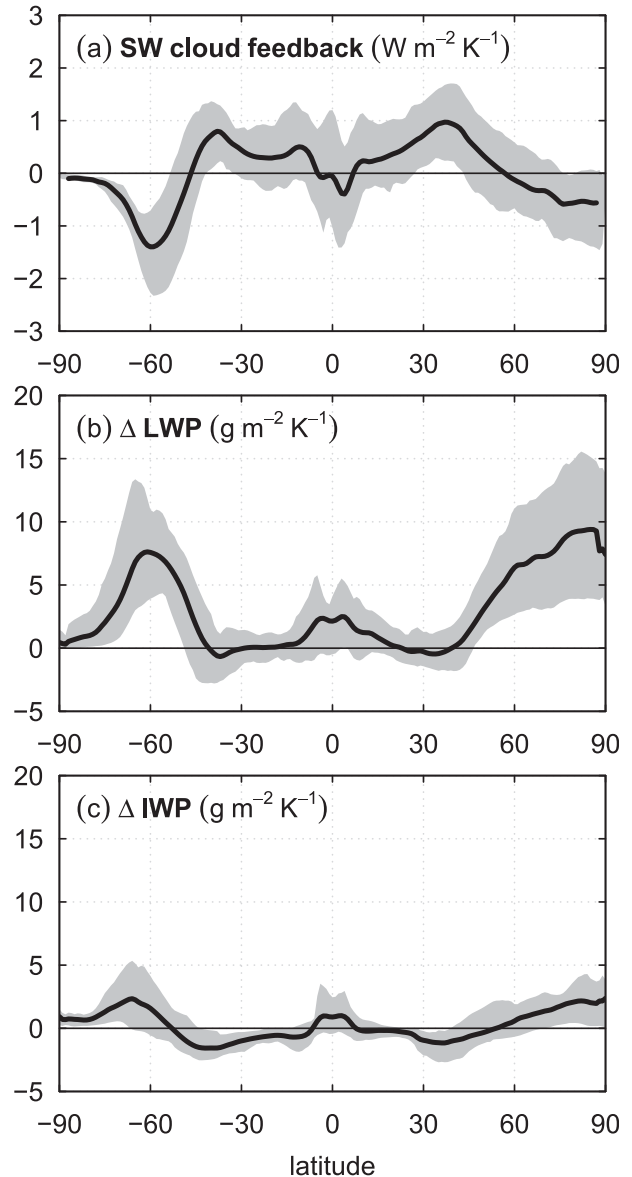

FIG. 1. Model responses (2050–99 minus 1950–99) in the RCP8.5 experiment of CMIP5, based on the first ensemble member of 32 models (Table B1): (a) SW cloud feedback, (b) change in gridbox-mean LWP, and (c) change in gridbox-mean IWP. In all panels, the black curves denote the multimodel mean response and the gray shading includes 75% of the models. The changes are normalized by the global-mean surface temperature increase in each model. The cloud feedback is calculated using the approximate partial radiative perturbation (APRP) method of Taylor et al. (2007), and includes rapid adjustments.

warming response (Kay et al. 2014; Ceppi et al. 2014; Ceppi and Hartmann 2015), so that the poleward shift of the storm tracks is unlikely to be a dominant contribution to the negative optical depth feedback.

The aim of this paper is to test the importance of mechanism 1 for the global warming response of cloud

water and the associated negative SW cloud feedback in climate models. In state-of-the-art climate models, the conversion rates between cloud liquid water, cloud ice, and precipitating particles are governed by the cloud microphysics scheme, where they are parameterized as functions of variables such as temperature, moisture, and ice nucleating aerosols. The relative amounts of cloud liquid water and ice are also influenced by the detrainment of condensate from convection, since the partitioning of detrained condensate between liquid and ice phases is often a simple function of temperature in climate models. In the next section, we present a methodology to quantify the contribution of cloud microphysics and convective condensate partitioning to the cloud water response to warming.

3. Model description and experimental setup

We run two climate models in aquaplanet configuration with prescribed sea surface temperature (SST) lower boundary conditions and perpetual equinox insolation. The models are AM2.1, developed at the Geophysical Fluid Dynamics Laboratory (Anderson et al. 2004), and the Community Earth System Model (CESM) version 1.2.1, of which we use the atmospheric component CAM5 (Hurrell et al. 2013; Neale et al. 2012). We choose an aquaplanet configuration because it is the simplest setup in which the mechanisms described in this paper can be studied. The symmetric, seasonally invariant boundary conditions also mean that meaningful results can be obtained with relatively short simulations. Following the aquaControl and aqua4K experiment protocol in CMIP5, we force our models with the Qobs SST profile (Neale and Hoskins 2000) and simulate the effects of global warming by applying a uniform 4-K SST increase. All experiments are run for a minimum of five years, after spinning up the model for a year, and all results presented in this paper are averages over both hemispheres. The models are run at a horizontal resolution of $2°$ latitude $\times$ $2.5°$ longitude (AM2.1) and $1.9° \times 2.5°$ (CESM-CAM5), with 24 and 30 vertical levels, respectively.

To understand the cloud water response to global warming in our models, we design a set of experiments to isolate the effect of changes in cloud microphysical rates and in the phase partitioning of convective condensate with warming. As we will show, the main impact comes from the sensitivity of microphysical process rates to changes in temperature, affecting the size of the reservoirs of cloud liquid water and ice in mixed-phase regions. Below we describe the relevant model physics and the experimental design in more detail.

a. Cloud microphysics schemes and partitioning of convective condensate

Both models in this study include a prognostic bulk microphysics scheme with separate variables for liquid water and ice, but they use different parameterizations. We summarize the main characteristics of each scheme here, and refer the reader to the cited literature for additional detail. The cloud microphysics in AM2.1 are single-moment (predicting liquid water and ice mixing ratios only) and are mainly based on Rotstayn (1997) and Rotstayn et al. (2000). The CESM-CAM5 microphysics scheme, described in Morrison and Gettelman (2008) and Gettelman et al. (2010), predicts two moments of the particle size distribution (mixing ratios and number concentrations) for liquid water and ice separately. CESM-CAM5's microphysics are more complex than those of AM2.1, including a much larger number of processes, particularly in the ice microphysics. Note that because both cloud microphysics schemes have separate prognostic equations for liquid water and ice, the fraction of total cloud water that is in the ice phase is not a simple explicit function of temperature. Rather, the relative amounts of liquid and ice result from the net effect of competing source and sink terms for each phase, whose rates depend on local thermodynamic conditions, aerosol concentrations, and other variables.

It is worth emphasizing that the cloud microphysical parameterizations apply only to the stratiform (large scale) cloud schemes. The convection schemes use highly simplified microphysics to calculate cloud condensate mixing ratios and convective precipitation rates. In both models used in this study, the partitioning of convective condensate into liquid and ice phases is based on a simple temperature threshold. In AM2.1, detrained convective condensate is assumed to be entirely liquid at temperatures higher than $-40°C$. By contrast, in CESM-CAM5 the fraction of frozen condensate is a linear function of temperature, varying between 0 at $-5°C$ and 1 at $-35°C$.

An important additional difference in the microphysics schemes between AM2.1 and CESM-CAM5 is in the treatment of snow. In AM2.1, cloud ice and snow are treated as a single species, whereas in CESM-CAM5 they are distinct. Snow in CESM-CAM5 is radiatively active, however (Neale et al. 2012), and is much more prevalent than cloud ice in midlatitudes, its vertically integrated mass being roughly 3 times that of cloud ice at $50°$ (not shown). Because of this difference in the treatment of snow, cloud ice mixing ratios appear to be considerably smaller in CESM-CAM5 compared to AM2.1. This difference should be kept in mind in the

TABLE 1. List of experiments described in this paper. The following abbreviations are used: PCond for the partitioning of convective condensate, Micro for microphysics, P for precipitation, and WBF for Wegener–Bergeron–Findeisen.

Experiment	Description	Processes involved (Tables A1 and A2)	
		AM2.1	CESM-CAM5
Micro$_{WBF}$	Perturb WBF process	WBF	WBF (liquid → ice and liquid → snow)
Micro$_P$	Perturb temperature-dependent microphysical processes involving precipitation	melting (ice → rain, snow → rain), riming	All processes in ice → snow, rain → snow, snow → rain, snow → snow, as well as accretion of liquid droplets by snow (PSACWSO)
Micro$_{nucl+frz}$	Perturb homogeneous and heterogeneous ice nucleation and homogeneous and heterogeneous freezing	Homogeneous freezing	Homogeneous nucleation, heterogeneous nucleation, homogeneous freezing, heterogeneous freezing (immersion and contact)
Micro	Perturb all temperature-dependent microphysical processes	All processes in Tables A1 and A2	
PCond	Perturb temperature threshold for partitioning of detrained convective condensate	Detrainment of convective condensate to the grid-scale environment	
Micro+PCond	Micro and PCond perturbations together	All processes in Micro and PCond	
SST+4K	Uniform 4-K SST increase	—	

interpretation of our results but does not affect the conclusions drawn in the paper.

Importantly, AM2.1 and CESM-CAM5 also differ in the role of aerosols for ice nucleation. In AM2.1, aerosol concentrations are prescribed, aerosol–cloud interactions are not represented, and ice nucleation is assumed to be homogeneous, occurring below −40°C only. At temperatures below freezing, however, much of the newly formed cloud liquid water is rapidly converted to ice through the Wegener–Bergeron–Findeisen (WBF) process (Wegener 1911; Bergeron 1935; Findeisen 1938), for which a minimum cloud ice mixing ratio is always assumed to exist to trigger the process. By contrast, CESM-CAM5 has a *prognostic* aerosol scheme and includes different types of ice-nucleating aerosols with varying activation temperatures, with heterogeneous nucleation possible below −5°C (Neale et al. 2012). The aerosol sources in CESM-CAM5 are set by default to real-world conditions of year 2000, and include zonal and meridional asymmetries due to land–sea distribution and anthropogenic sources, inconsistent with the aquaplanet configuration. These inhomogeneities introduce an asymmetry in the LWP distribution, with Northern Hemisphere values about 25% larger compared to the Southern Hemisphere at 50°; there are no obvious asymmetries in IWP, however (not shown). While real-world aerosol sources are inconsistent with the aquaplanet configuration, they also make our results more comparable with more realistic CMIP5 experiments.

b. Experimental setup

We perform a series of simulations to isolate the effects of changes in temperature on the cloud microphysical rates and on the phase partitioning of convective condensate, and quantify their impact on cloud liquid water and ice mixing ratios. The experiments are listed and described in Table 1, with additional details in appendix A. Our goal here is to test the hypothesis that the direct effect of warming on microphysical rates can reproduce important aspects of the global warming response of cloud condensate, without directly perturbing other potentially relevant processes such as atmospheric circulation, moisture convergence, radiative heating rates, aerosol concentrations, or the temperature dependence of the moist adiabat. We test this idea by simply increasing temperature by 4 K in the relevant sections of the code.[1] Note that SSTs are kept at their control value in all of these experiments except SST+4K.

The temperature perturbation affects only those microphysical processes that involve the ice phase; the

---

[1] Increasing temperature by 4 K at all atmospheric levels ignores the increase in static stability that occurs in the case where SSTs are increased, which produces stronger warming at upper levels. However, in the middle and high latitudes most of the cloud water is found in the lower troposphere (as shown later in the paper), where the actual temperature increase is very close to 4 K.

perturbed processes are discussed in appendix A (see Tables A1 and A2). Perturbing temperature can affect ice-phase microphysical processes in two ways. First, all processes producing (destroying) ice occur only below (above) a given temperature threshold, so increasing temperature modifies the spatial occurrence of those processes, as isotherms shift in space. Second, in CESM-CAM5 a few ice-forming process rates are explicit functions of temperature. This includes processes such as heterogeneous freezing as well as ice multiplication via rime-splintering (Neale et al. 2012). It should be noted that the perturbed processes involve conversions between liquid water, ice, and precipitation (and subsequent melting/freezing of hydrometeors). Conversions between vapor and cloud condensate are generally not perturbed, with only two exceptions in CESM-CAM5, described in appendix A.

4. Results

We begin by describing the aquaplanet model responses to a 4-K SST increase (the SST+4K experiment in Table 1). The SW cloud radiative effect (CRE) and LWP responses, shown in Figs. 2a and 2b, look qualitatively similar to the mean RCP8.5 response in CMIP5. The aquaplanet simulations capture the negative cloud feedback in the middle to high latitudes, as well as the associated LWP increase. Relative to the control values, the LWP increase at 50° is about 15% K^{-1} in CESM-CAM5 and 20% K^{-1} in AM2.1, well in excess of the expected adiabatic water content increase (see e.g., Gordon and Klein 2014, Fig. 2b).

By contrast, the IWP responses are strikingly different poleward of 40° (Fig. 2c), with AM2.1 featuring an increase and CESM-CAM5 a decrease (this response remains qualitatively similar if snow is included in the CESM-CAM5 IWP). Finally, cloud amount (fractional coverage) tends to decrease in the middle to high latitudes (Fig. 2d). Cloud amount changes also explain most of the SWCRE response equatorward of 40°, consistent with the findings of Zelinka et al. (2012) for CMIP3 models. In the middle and high latitudes, the cloud amount and IWP responses likely also explain some of the differences in the SW CRE response between the models, particularly the weaker negative SW feedback in CESM-CAM5 compared to AM2.1. Despite these differences, the SW CRE response poleward of 40° appears to be dominated by the LWP increase, consistent with the stronger radiative effect of liquid droplets compared to ice crystals, which have a larger effective radius.
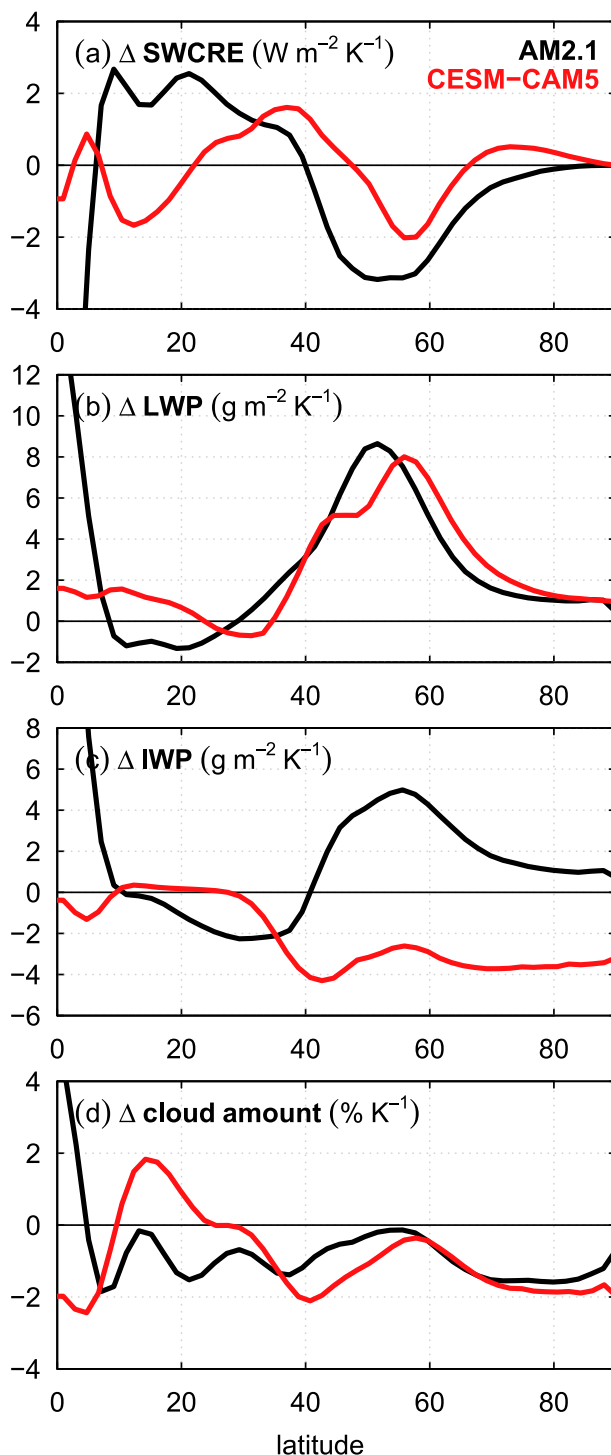

FIG. 2. Aquaplanet model responses upon a 4-K SST increase, all normalized by the surface warming: (a) SW cloud radiative effect, (b) LWP, (c) IWP, and (d) cloud amount (or fractional coverage). Black and red curves denote AM2.1 and CESM-CAM5, respectively.
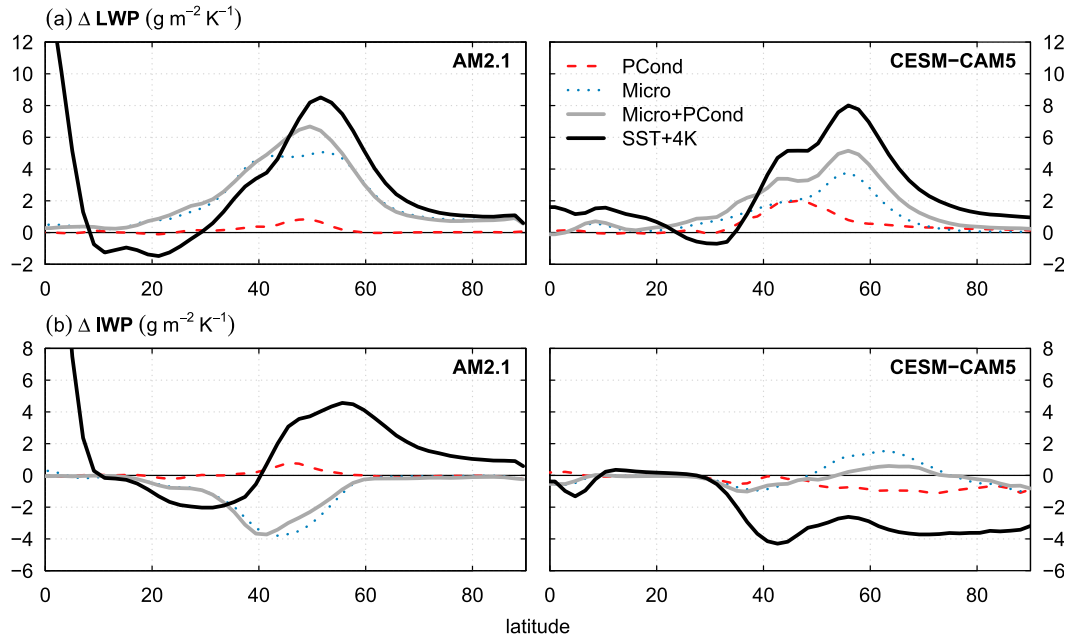
FIG. 3. Gridbox-mean (a) LWP and (b) IWP responses in the PCond (red dashed), Micro (blue dotted), Micro+PCond (thick gray), and SST+4K (thick black) aquaplanet experiments (see Table 1 for a description). All responses are normalized assuming a 4-K warming.

While we show the cloud amount response in Fig. 2 for completeness, in the remainder of this paper we will focus on the cloud liquid water and ice responses and their relationship to microphysical processes and the partitioning of convective condensate. Although we only show gridbox-mean (as opposed to in-cloud) condensate changes throughout the paper, we have verified that cloud amount changes cannot explain the cloud water changes shown in this paper; in other words, the LWP and IWP responses mainly result from changes in in-cloud mixing ratios, rather than from cloud amount changes. This is consistent with the occurrence of large LWP increases in midlatitudes despite weak decreases in cloud amount, as shown in Fig. 2.

a. Cloud microphysics and partitioning of convective condensate

Figure 3 shows the LWP and IWP responses in the PCond, Micro, and Micro+PCond experiments (see Table 1), and compares them with the SST+4K response. All results in this and subsequent figures are normalized by the temperature change, assuming a 4-K warming for the Micro and PCond experiments. We begin by discussing the PCond case (red dashed curves in Fig. 3). Increasing temperature by 4 K in the partitioning of convective condensate yields a relatively small LWP increase (Fig. 3a), although the response is about twice as large in CESM-CAM5 compared to

AM2.1. The smaller response in AM2.1 can be related to the choice of temperature threshold for the phase partitioning, as explained in section 3a. The very low temperature threshold in AM2.1 means that only a small fraction of the detrained convective condensate can be converted to ice compared to CESM-CAM5, since little cloud water is available at the low threshold temperature in AM2.1; this results in a lower sensitivity to a temperature increase. In addition, the choice of a 30-K temperature ramp for the phase partitioning of convective condensate (as opposed to the step function choice in AM2.1) means that a much wider range of temperatures can experience the effect of the 4-K warming in CESM-CAM5. However, part of the difference might also result from smaller convective detrainment rates in AM2.1 (typically by a factor of 2 to 4 in the middle to high latitudes) compared to CESM-CAM5 (not shown).

The IWP response to the PCond perturbation is also modest in both models (Fig. 3b). Somewhat counterintuitively, IWP mostly *increases* in AM2.1 around the midlatitudes; we believe this is a result of the increased cloud liquid water mixing ratio, some of which is subsequently converted to ice through microphysical processes, rather than a direct response to the temperature perturbation. As will be shown later in this paper, in AM2.1 most of the cloud liquid water in mixed-phase clouds is converted to ice before precipitating.
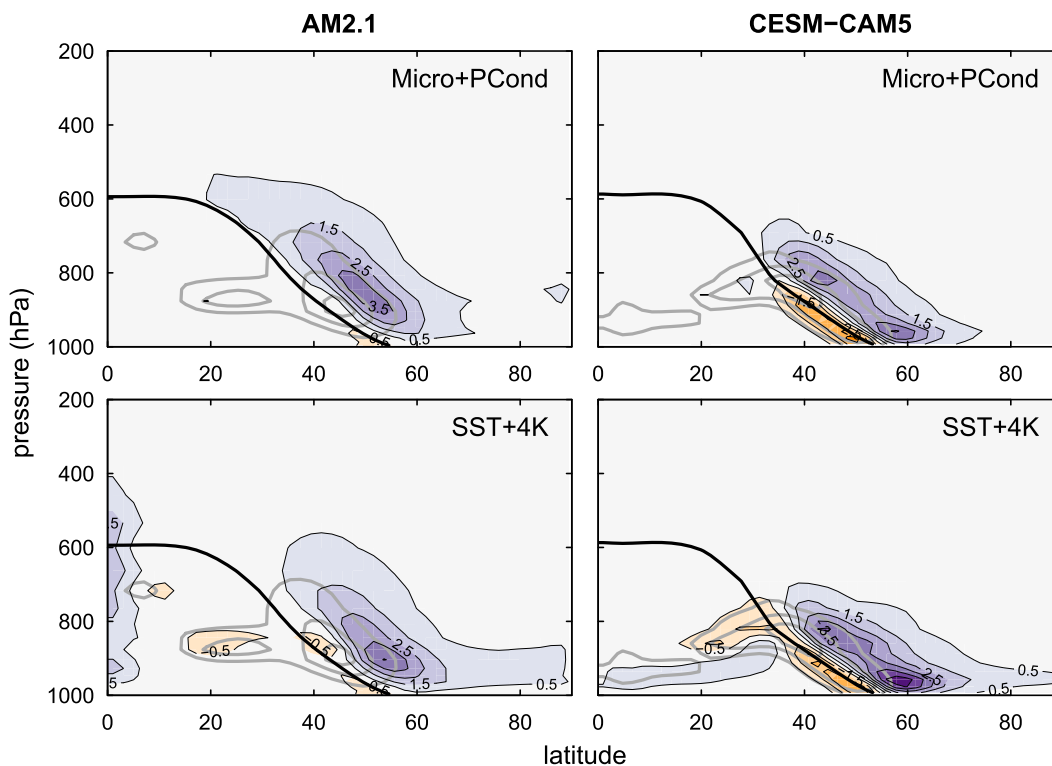
FIG. 4. Changes in gridbox-mean cloud liquid water mixing ratio (shading, in mg kg^{-1} K^{-1}) as a function of latitude and pressure in the Micro+PCond and SST+4K aquaplanet experiments. Thick gray contours represent the control climatology (contours every 10 mg kg^{-1}), while the thick black curve denotes the melting line (0°C isotherm) in the control experiment.

The microphysical perturbations explain a much larger fraction of the LWP changes in both models (Fig. 3a, blue dotted curves). Around 50°, Micro produces about two-thirds of the SST+4K response in AM2.1, and close to half in CESM-CAM5. The LWP responses in Micro also capture the general latitude dependence of the SST+4K response remarkably well, peaking between 50° and 60°. In contrast, the IWP responses in Micro do not seem to bear much resemblance to the SST+4K response. However, we will show later in this section that key aspects of the vertical structure of the cloud ice response are indeed reproduced by the Micro experiments.

Applying the Micro and PCond forcings together (thick gray curves in Fig. 3) yields LWP changes that are even closer to the SST+4K response, generally explaining more than two-thirds of the response around the midlatitudes. For both LWP and IWP, the Micro and PCond perturbations are nearly additive. The resemblance between the Micro+PCond and SST+4K cloud liquid water responses is even more striking when considering the vertical structure of the cloud water mixing ratio changes (Fig. 4). In both models, most of the response occurs in a band upward and poleward of the freezing line (black curves in Fig. 4). The liquid water increase also occurs just upward and poleward of the climatological distribution (gray contours in Fig. 4), resulting in a net increase and poleward expansion of the climatological LWP. The vertical structure and general temperature dependence of the cloud liquid water response to warming is very consistent with the results of Senior and Mitchell (1993), Tsushima et al. (2006), and Choi et al. (2014), all of whom also noted the coupling between the freezing isotherm and the cloud liquid water response. This coupling suggests an important control of temperature on microphysical process rates and the cloud liquid water reservoir, which we will further explore in the next section.

The vertical cross sections of the cloud ice mixing ratio response (Fig. 5) also show that the Micro+PCond experiment does capture a significant part of the cloud ice response to warming. In AM2.1, a large cloud ice decrease occurs right above the freezing line, where ice production from liquid water is suppressed upon warming. However, the SST+4K experiment features an additional increase in cloud ice at higher altitudes that is mostly absent from Micro+PCond, explaining the discrepancy between the vertically integrated responses
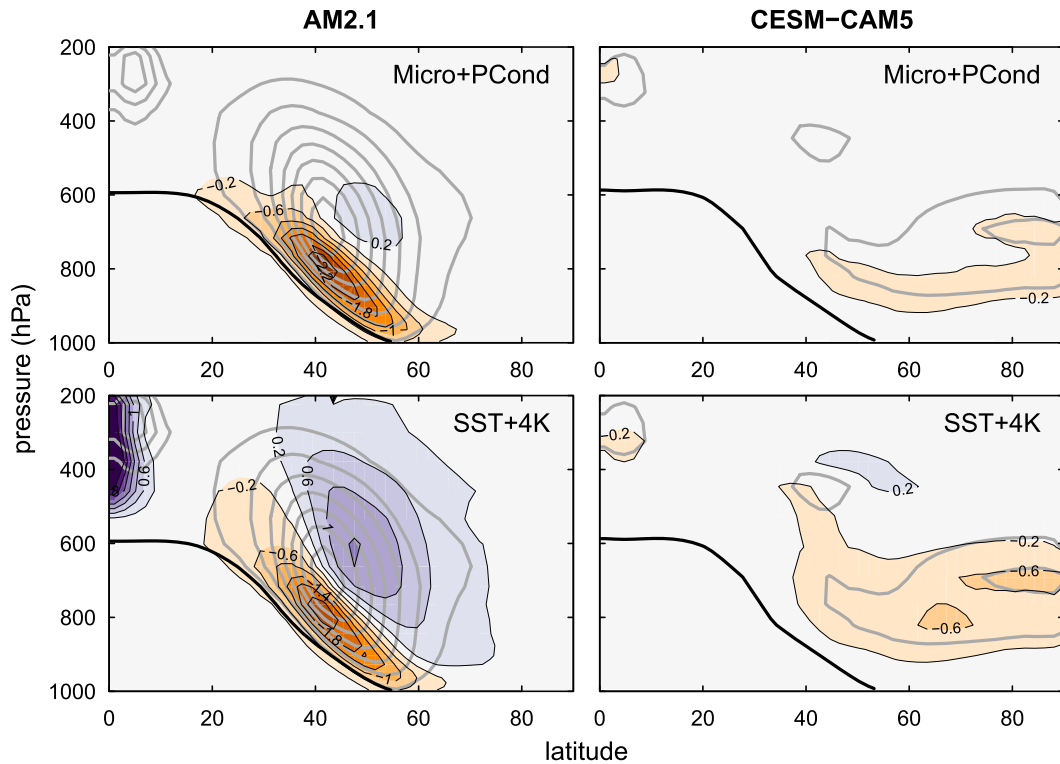
FIG. 5. As in Fig. 4, but for changes in cloud ice mixing ratio. The contour interval for the climatology (thick gray contours) is 3 mg kg^{-1}.

shown in Fig. 3. In CESM-CAM5, there is no large ice response near the freezing line, consistent with the climatological cloud ice distribution being centered farther poleward and away from the freezing isotherm compared to AM2.1 (gray contours in Fig. 5). (If snow and cloud ice are counted together as in AM2.1, however, a large decrease near the freezing line does appear, consistent with AM2.1.) While the Micro+PCond experiment does produce a decrease in cloud ice, it underestimates the response compared to SST+4K; much of this difference appears to result from different changes in cloud amount in the region of cloud ice decrease, since the in-cloud mixing ratios indicate a more consistent decrease in both experiments (not shown).

Taken together, the results presented in this section show that the cloud liquid water content of mixed-phase clouds is strongly controlled by the temperature dependence of microphysical process rates, and to a lesser degree by the temperature dependence of the partitioning of convective condensate. This suggests that a large fraction of the global warming response of cloud liquid water can be attributed to the direct effect of warming on cloud microphysics, rather than other processes such as adiabatic increases in moisture content with warming, changes in moisture convergence, or

changes in radiative heating rates, at least in the two models considered in this study. While important aspects of the cloud ice response are also explained by the microphysics and convective condensate partitioning perturbations, additional processes would need to be considered to capture the full global warming response of cloud ice in our two models. In the next section, we study the microphysical processes in more detail and explain how their temperature and moisture dependence controls the cloud liquid water content.

b. Microphysical processes

As discussed in section 3, the cloud microphysics schemes in AM2.1 and CESM-CAM5 are prognostic, so that the schemes calculate conversion rates between water vapor, cloud liquid water, cloud ice, and precipitation, based on physical parameterizations of the relevant processes. Thus, the liquid water and ice contents of clouds are ultimately determined by the relative efficiency of their respective sources and sinks. From this perspective, the response of cloud liquid water and ice to warming can be thought of as resulting from changes in the relative efficiencies of the corresponding source and sink terms.

The microphysical conversions are depicted schematically in Fig. 6, using the rates output directly by the
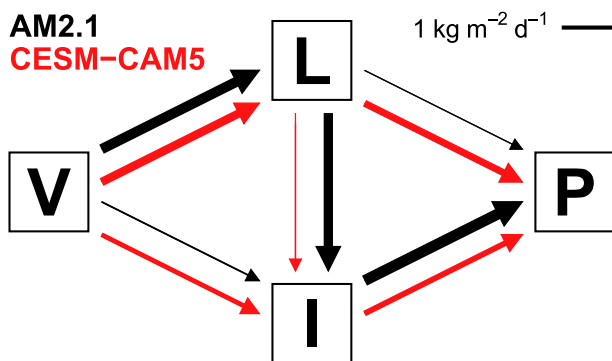
FIG. 6. Net vertically integrated conversion rates between vapor (V), cloud liquid water (L), cloud ice (I), and precipitation (P) in the aquaplanet control climatology. The conversions from V to L and V to I include contributions from large-scale condensation (in the cloud macrophysics scheme) and detrainment from convection, while all other conversions shown here occur in the cloud microphysics only. The arrow width is proportional to the net conversion rate. Black and red arrows denote AM2.1 and CESM-CAM5, respectively. Reevaporation of precipitation is omitted.

model. The arrows in Fig. 6 point in the direction of the net vertically integrated conversion rate at 50°, with the arrow thickness proportional to the conversion rate. The mean rates of individual conversion processes are also provided in the appendix (Tables A1 and A2). (Note that the fluxes between vapor and condensate are dominated by large-scale condensation from the cloud *macrophysics* scheme, as well as condensate detrainment from convection, rather than by microphysical processes.) The schematic shows that in both models, there is a net source of cloud liquid water from condensation, and net sinks from conversion of liquid water to ice and precipitation. However, the relative importance of the liquid water sinks differs greatly between the models: whereas in AM2.1 almost all of the liquid water is converted to ice before precipitating, in CESM-CAM5 most of the liquid water is directly converted to precipitation, with little net conversion to ice. The varying importance of the sources and sinks of cloud liquid water and ice suggests that the microphysical processes responsible for the cloud water response to warming may be different in the two models.

The intermodel differences in Fig. 6 partly reflect different philosophies in the implementation of certain microphysical processes. For example, growth of ice crystals through the WBF process is treated as a flux from liquid to ice in AM2.1, while in CESM-CAM5 it may be treated as a flux from liquid to ice or vapor to ice, depending on the availability of liquid water in the grid box (see Gettelman et al. 2010). In reality, however, this is a multistep process involving condensation,

reevaporation, and deposition onto ice, but these multiple steps are represented in neither of the schemes. In addition, the conversion of liquid water to snow is treated as a precipitation-forming process in CESM-CAM5; in AM2.1, however, the same phenomenon would be described as a conversion of liquid water to ice, since no distinction is made between ice and snow inside clouds. This likely contributes to the fact that the overall conversion efficiency of liquid water to ice is much smaller in CESM-CAM5 than in AM2.1. In summary, it is important to keep in mind that differences in the fluxes in Fig. 6 partly result from somewhat arbitrary choices in the representation of the microphysics.

To gain additional insight into the mechanisms of the microphysical response to warming, we group the microphysical processes into three categories, and perturb temperature in each of them separately. We consider the WBF process (Micro$_{WBF}$), thought to be one of the dominant mechanisms converting liquid water to ice in climate models (e.g., Storelvmo and Tan 2015); homogeneous and heterogeneous ice nucleation and freezing (Micro$_{nucl+frz}$); and all precipitation processes (Micro$_P$). The latter category includes the conversion of cloud condensate to rain or snow, as well as the subsequent freezing or melting of precipitating particles. The three experiments are described in Table 1, and details of the processes involved in each experiment are provided in Tables A1 and A2. Together, these three experiments include all of the processes in Tables A1 and A2, except for ice melting in CESM-CAM5 (MELTO in Table A2; we have verified this has no impact on the results).

Figure 7 shows the separate contributions of Micro$_{WBF}$, Micro$_P$, and Micro$_{nucl+frz}$ to the LWP response to warming. In both models, Micro$_{WBF}$ is the largest contribution to the LWP increase, explaining about half or more of the total Micro LWP response. This is consistent with the WBF process being the dominant conversion mechanism from liquid water to ice (Tables A1 and A2). Upon warming, the conversion efficiency of liquid water to ice is reduced, leading to an increase of the liquid water reservoir until the net conversion rate of liquid water to ice is sufficiently large to balance the source terms. In both models, the same perturbation leaves the IWP nearly unchanged (Fig. 7b), because the increase in cloud liquid water balances the decreased conversion efficiency of liquid water to ice.

The second largest impact on the LWP response comes from the precipitation processes, although the impacts are different in the two models (orange dotted curves in Fig. 7). In AM2.1, Micro$_P$ produces a substantial LWP increase, while also causing all of the IWP decrease seen in the Micro experiment. The LWP increase results from riming being suppressed near the
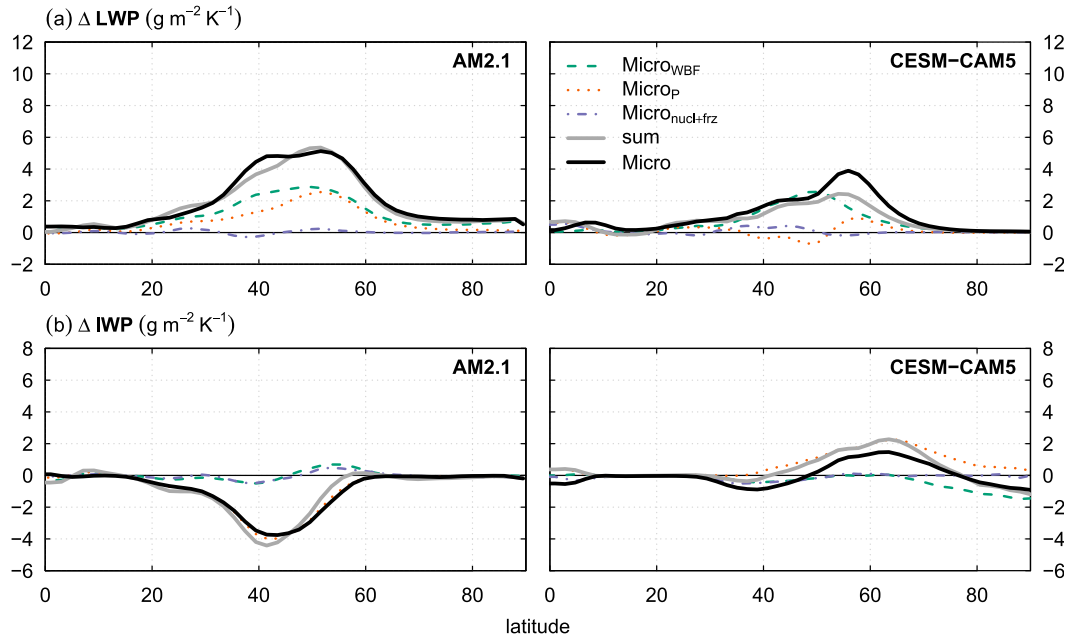
FIG. 7. As in Fig. 3, but showing the LWP and IWP changes in Micro$_{WBF}$, Micro$_P$, and Micro$_{nucl+frz}$.

freezing line upon warming.[2] The IWP decrease results from the fact that in the AM2.1 cloud microphysics, all melting cloud ice is assumed to convert to rain rather than cloud liquid water, so ice melting is regarded as a precipitation process here; the temperature increase thus forces the melting of ice in regions near the freezing line.

By contrast, in CESM-CAM5 the impact of precipitation processes on LWP is small (Fig. 7a, right). However, the vertically integrated cloud water changes are somewhat misleading, since the precipitation processes in Micro$_P$ explain most of the vertical structure of the cloud water changes shown in Fig. 4, including the weak decreases near and below the freezing line; the cloud water response in Micro$_P$ thus consists of a vertical dipole (not shown). In addition, we have tested in supplementary experiments that the WBF and precipitation processes interact with each other to amplify the LWP response to warming. For instance, an experiment that includes perturbing both WBF and precipitation processes yields a LWP increase similar to the full Micro

response (not shown), despite the fact that the sum of Micro$_{WBF}$ and Micro$_P$ is smaller. Furthermore, the processes in Micro$_P$ are the dominant contribution to the IWP response in the Micro experiment in CESM-CAM5 (Fig. 7b, right). Thus, the importance of the processes in Micro$_P$ should not be underestimated, even if the LWP response appears small in CESM-CAM5.

Finally, the contributions of ice nucleation and freezing to the LWP and IWP responses are negligible in both models (purple dash-dotted curves in Fig. 7). This is consistent with the inefficiency of these processes in the control climate (Tables A1 and A2). Thus, the main finding of this section is that cloud liquid water increases with warming result mainly from the suppression of ice microphysical processes that deplete liquid water by converting it to ice or precipitation. The resulting increase in condensed water with warming is consistent with the notion that clouds containing ice precipitate more efficiently (Senior and Mitchell 1993; Tsushima et al. 2006; Gordon and Klein 2014; Komurcu et al. 2014). This suggests that an accurate parameterization of ice growth and precipitation processes is crucial for the representation of the climatology and forced response of cloud water content in climate models.

5. Temperature–LWP relationship in CMIP5 models and observations

We have shown that the temperature dependence of microphysical process rates and of the phase partitioning

---

[2] For AM2.1, riming is included as a precipitation process in Micro$_P$ since no distinction is made between ice and snow within the cloud. Also, changes in ice melting strongly affect the occurrence of the riming process, since it can only occur in the presence of cloud ice; it is therefore a sensible choice to combine ice melting and riming in one experiment (Table 1). We regard riming in AM2.1 as the equivalent to accretion of cloud liquid water by snow in CESM-CAM5 (Tables A1 and A2).

of convective condensate explains most of the cloud liquid water increase in the middle and high latitudes in two climate models, AM2.1 and CESM-CAM5. In this section, we present evidence supporting this conclusion in other climate models and observations. One key aspect of our results is that temperature alone controls most of the LWP changes in mixed-phase clouds. If this is generally the case in models and observations, then the following two hypotheses can be made:

1) Cloud liquid water and temperature are robustly positively correlated in the middle to high latitudes.
2) The cloud liquid water response to unforced (e.g., seasonal) temperature variations is similar to the forced response.

While a dependence of LWP on temperature would also be expected if cloud liquid water increases adiabatically with warming, we will show that a robust temperature–LWP relationship exists only in the middle to high latitudes in models and observations, coincident with the mixed-phase regime. Furthermore, the magnitude of this temperature–LWP relationship varies considerably among models, which cannot be ascribed to simple thermodynamic arguments such as the increase in adiabatic cloud water content. These results suggest an important role for microphysical ice-phase processes in the LWP response to warming.

We test our two hypotheses by calculating correlation and regression coefficients for monthly mean temperature–LWP relationships in models and observations. The data include output from the historical experiments of 32 CMIP5 models (Table B1), as well as satellite LWP retrievals for 1989–2008 (O'Dell et al. 2008) combined with reanalysis temperature from ERA-Interim (Dee et al. 2011). Since we do not remove the seasonal cycle from the data, most of the joint LWP and temperature variability reflects the annual cycle. For simplicity, we use temperature averaged between the 500- and 850-hPa levels, the layer containing the bulk of the cloud liquid water in most models (not shown), and average the data zonally before calculating the correlations and regressions. Because satellite LWP observations are only available over the oceans, we remove land grid points from the model data to ensure that the results are comparable between models and observations, but note that the model results are very similar if land areas are included (not shown).

In agreement with hypothesis 1, models and observations feature strong positive correlations between temperature and LWP in the middle- and high-latitude regions in both hemispheres (Fig. 8a). The correlations are particularly high in the observations, peaking at 0.95 near 50°. The latitude beyond which the correlations

become positive varies considerably among models, and may reflect differences in the meridional extent of mixed-phase regions. It should also be noted that the observations feature positive LWP–temperature correlations at lower latitudes than the majority of the models. Over the Southern Ocean poleward of 60°S, the LWP–temperature correlation becomes lower in observations than in models; it is unclear whether this reflects a different LWP–temperature relationship in the observations, or whether it is related to measurement errors, for example over sea ice regions.

Consistent with the positive correlation coefficients, all models (as well as the observations) produce a LWP increase around the midlatitudes for increasing lower-tropospheric temperature, although there is substantial intermodel variability in the magnitude and meridional structure of the LWP regression coefficients (Fig. 8b). The strong positive LWP–temperature relationships are consistent with the results of Gordon and Klein (2014), who found positive condensed water path–temperature relationships in models for low clouds with cloud-top temperatures below freezing. Earlier studies based on in situ observations also found similar relationships in cold clouds (Feigelson 1978; Gultepe and Isaac 1997). We believe that regions of positive regression and correlation coefficients correspond to regions where clouds are predominantly mixed-phase, and where LWP is therefore strongly influenced by temperature-dependent ice-phase microphysical processes.

Comparing models with observations, we note that models are in general agreement with the observed LWP–temperature relationship, especially in the Northern Hemisphere (Fig. 8b). However, many models largely overestimate the LWP increase with warming between 50° and 70°S; this may result from most models overestimating the effective glaciation temperature and underestimating the fraction of supercooled liquid, which is linked to a larger LWP response to warming (McCoy et al. 2015; Cesana et al. 2015). This implies that models may overestimate the contribution of microphysical processes to the LWP increase with warming. Additional research based on remotely sensed data and in situ observations will be needed to quantify the efficiency of ice-phase microphysical processes and their contribution to the cloud feedback in the real world. Nevertheless, a key result is that the observed LWP–temperature relationships support the idea of a negative SW cloud feedback in the middle to high latitudes, driven by increases in cloud liquid water content. We further discuss this idea below.

The LWP response in RCP8.5 (normalized by the local warming in each model) looks remarkably similar to the regression coefficients (cf. Figs. 8b and 8c), both in
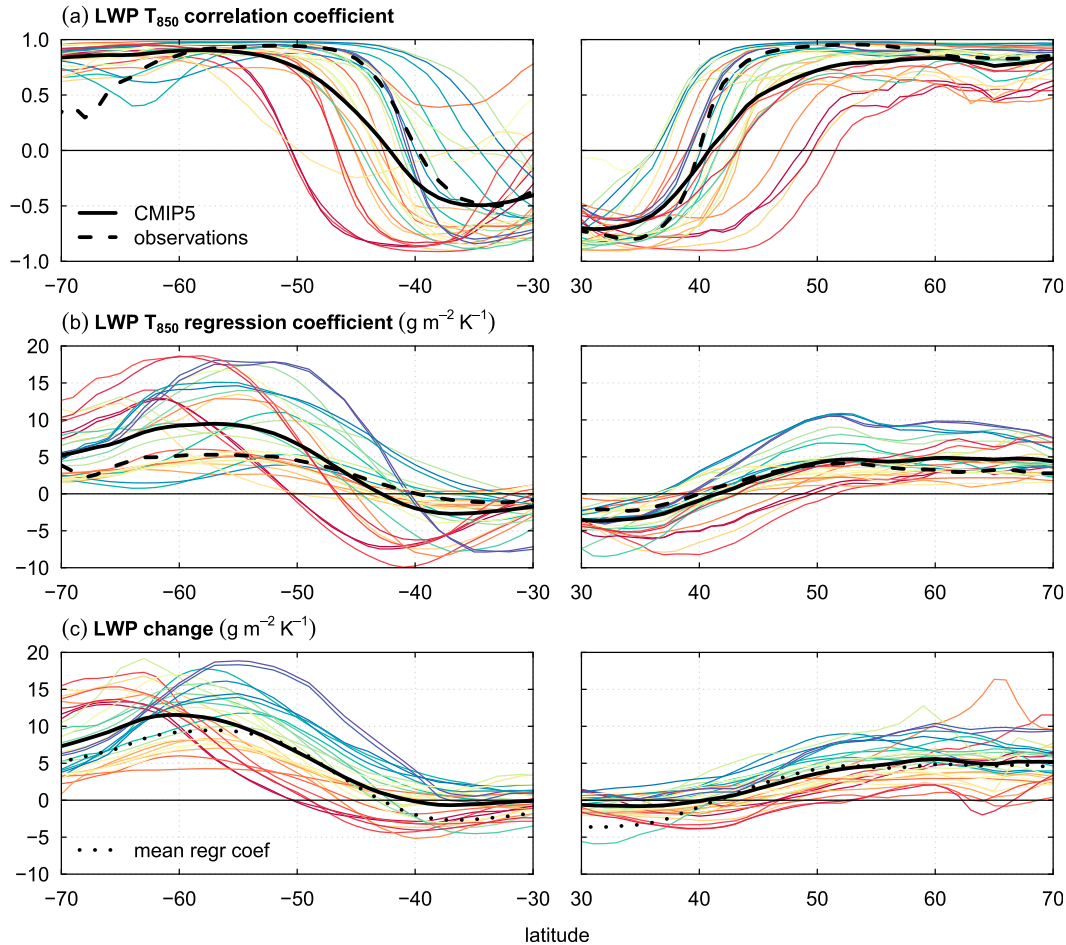
FIG. 8. Relationships between lower-tropospheric temperature (averaged between 500 and 850 hPa) and LWP in CMIP5 models and observations: (a) correlation between monthly mean, zonal-mean LWP and temperature in the historical experiment of CMIP5 and observations; (b) as in (a), but for the regression coefficient of LWP onto temperature; and (c) RCP8.5 minus historical LWP response normalized by the local warming in each model. In all panels, colored curves represent individual CMIP5 models with the multimodel mean in thick black, and the dashed black curve denotes observations. The model curves are colored according to the LWP change at 50°S from (c). For CMIP5 models, the historical and RCP8.5 periods are 1980–99 and 2080–99, respectively. For the observations, LWP satellite observations for 1989–2008 (O'Dell et al. 2008) are combined with ERA-Interim reanalysis temperature (Dee et al. 2011). Because LWP satellite observations are available over oceans only, all land grid points are excluded from the analysis for both models and observations.

terms of magnitude and meridional structure of the response. The relative order of the models is also similar, so that models with more positive regression coefficients tend to produce a larger LWP increase with warming, and vice versa. In relative terms, the multimodel mean LWP increase varies between about 5% K^{-1} at 50° and 15% K^{-1} at 70°N/S; these increases are therefore comparable to or larger than those expected from adiabatic theory (Betts and Harshvardhan 1987; Gordon and Klein 2014).

The good agreement between the LWP regression coefficients and forced responses across models is confirmed by plotting the two quantities against each other,

averaged over 45°–70°N/S (Fig. 9); the values are well correlated in both hemispheres (0.59 and 0.64 in the Northern and Southern Hemispheres, respectively). As expected, the two CMIP5 models that share the AM2.1 atmospheric component behave very similarly. Gordon and Klein (2014) found a similar time-scale invariance in the relationship between total cloud water content and temperature in a smaller set of climate models. This result provides hope that it may be possible to constrain the SW cloud feedback in the middle to high latitudes using observed LWP–temperature relationships as validation targets for model cloud microphysics schemes. The results in Fig. 8b also suggest that the negative SW
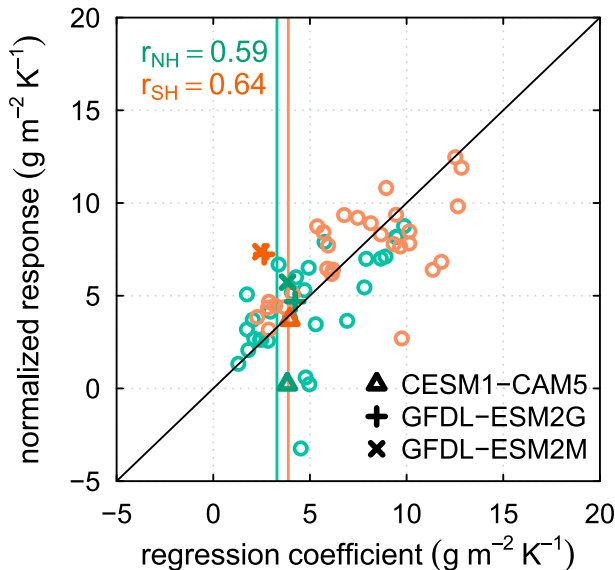
FIG. 9. LWP change averaged over 45°–70°N/S in the RCP8.5 experiment (normalized by the lower-tropospheric temperature change) vs the historical regression coefficient of LWP over lower-tropospheric temperature. Both *x* and *y* values are calculated as in Figs. 8b and 8c. Northern and Southern Hemisphere values are shown in red and blue, respectively. The regression coefficients from observations are shown as vertical bars. The one-to-one line is shown for reference.

cloud feedback predicted by models may be too large, especially over the Southern Ocean. We will explore these ideas in future work.

6. Summary and conclusions

A robust feature of global warming model experiments is a negative shortwave cloud feedback in the middle to high latitudes, driven by an optical thickening of the clouds associated with liquid water path (LWP) increases. We investigate the processes involved in the LWP response by perturbing temperature in the cloud microphysics schemes of two climate models in aquaplanet configuration, GFDL AM2.1 and CESM-CAM5, both of which have separate prognostic equations for liquid water and ice. We demonstrate that most of the LWP increase is a direct response to warming through a decrease in the efficiency of liquid water sinks, resulting in a larger reservoir of cloud liquid water. This occurs because temperature-dependent ice-phase microphysical processes are suppressed upon warming, reducing the efficiency of precipitation and Wegener–Bergeron–Findeisen (WBF) conversion to ice, the two main microphysical sinks for liquid water. An additional smaller contribution to the LWP increase comes from the phase partitioning of detrained convective condensate, which

is based on a simple temperature threshold in both models. Taken together, the microphysics and the partitioning of convective condensate explain about two-thirds of the LWP response to increasing SST in CESM-CAM5, and an even higher fraction in AM2.1.

While important aspects of the cloud ice response to warming are also reproduced in our experiments with perturbed microphysics, changes in ice water path (IWP) with increasing SST are not quantitatively predicted by increasing temperature in the cloud microphysics alone. Our two models also disagree on the IWP response to SST increase. This result is consistent with the IWP response being much less robust than the LWP response in RCP8.5 simulations of CMIP5 models. However, the larger radiative impact of small liquid droplets (compared to relatively large ice crystals) means that the shortwave cloud feedback is primarily determined by the LWP response.

In support of the conclusions drawn from our model experiments, we show that a robust positive relationship between temperature and LWP exists in both models and observations. This positive relationship occurs only in the middle and high latitudes, where mixed-phase clouds are expected to occur. Interestingly, the model-specific temperature–LWP relationships from the annual cycle are reflected in the different LWP responses to global warming, so the temperature dependence of LWP in mixed-phase regions appears to be largely time-scale invariant. This provides hope that observed relationships can provide a constraint on future LWP increases and on the associated shortwave cloud feedback.

Although models and observations all agree on LWP increasing with warming in mixed-phase cloud regions, most models appear to overestimate the LWP sensitivity to temperature compared with satellite observations. This may be because models overestimate the efficiency of ice-phase microphysical processes and do not maintain enough supercooled liquid in the historical climate. Additional work will therefore be necessary to confirm the relevance of cloud microphysics to the forced LWP response and the associated SW cloud feedback in the real world. The model biases in the LWP sensitivity to warming could imply an overly negative SW cloud feedback in high latitudes, with possible important implications for the representation of Arctic warming in models (Tselioudis et al. 1993).

Our results indicate that a fraction of the LWP response cannot be ascribed to a decrease in the efficiency of cloud liquid water sinks with warming. This is unsurprising, since it is to be expected that the liquid water *sources* might also respond to warming. Processes likely to also contribute to the LWP increase include

1) the increase in the temperature derivative of the moist adiabat, causing the adiabatic cloud water content to go up in saturated updrafts; and

2) the general increase in radiative cooling as the atmosphere becomes more emissive with warming, which must be balanced by enhanced latent heating and precipitation, at least on global scales.

Both of these effects would be expected to yield an enhanced rate of formation of cloud water as the atmosphere warms. Based on our results, however, changes in the liquid water sink terms exert a stronger control on the LWP response to warming, at least in our two models. While we noted that most models appear to overestimate the importance of microphysical processes in the LWP response to warming, the sensitivity of cloud water content to temperature in AM2.1 and CESM-CAM5 is near or below average compared to other climate models, and close to observations (Fig. 9).

Atmospheric circulation changes could also affect cloud water content. However, a regression analysis of LWP and IWP on zonal-mean jet latitude indicated that this is unlikely to be a major effect in our two models (not shown), as the cloud water changes associated with jet variability are small. This appears consistent with previous work showing the much larger impact of thermodynamic effects on cloud-radiative properties compared to dynamical effects (Ceppi and Hartmann 2015).

Our results suggest two important directions for future research. First, improved global-scale observations of cloud properties are needed to develop observational constraints on climate model behavior. For example, large uncertainties in cloud ice observations exist (e.g., Heymsfield et al. 2008), making an accurate estimation of model biases difficult. Second, an improved representation of ice-phase microphysical processes appears to be crucial to reduce the large model errors in both the present-day climatology and future response of condensed cloud water (Choi et al. 2014; Komurcu et al. 2014). In situ measurements and laboratory experiments will likely be necessary to constrain the model climatologies and improve current parameterization schemes. Progress on those issues will ultimately contribute to reducing the uncertainty in the cloud feedback, and will alleviate pervasive climatological biases associated with midlatitude clouds (Hwang and Frierson 2013; Ceppi et al. 2012).

APPENDIX A

Description of the Model Experiments

To ensure future reproducibility of our results, we provide additional details on our experiments in this appendix. As described in section 3b, the perturbation consists of applying a uniform 4-K temperature increase at all atmospheric grid points in the cloud microphysics schemes of our two models, while the rest of the model physics as well as the dynamics modules experience the "real" temperature. In addition to the temperature-dependent processes, the WBF mechanism (Wegener 1911; Bergeron 1935; Findeisen 1938), which converts cloud liquid water to ice or snow, also depends on the difference between saturation vapor pressure over liquid water (e_{sl}) and over ice (e_{si}), and this difference is directly related to temperature. For this process only, we perturb e_{sl} and e_{si} consistent with a 4-K warming, following the Clausius–Clapeyron relationship. Other temperature-dependent terms in the WBF process rate calculation [Rotstayn et al. 2000, their Eqs. (2)–(5); Morrison and Gettelman (2008, their Eq. (21)] are also adjusted for a 4-K warming.

Tables A1 and A2 list the microphysical processes that are perturbed. In AM2.1, these processes are found in the strat_cloud.f90 source file; in CESM-CAM5, the relevant source file is micro_mg1_0.F90. All of the perturbed processes involve the ice phase, and can therefore occur only within specific temperature ranges. The overall effect of increasing temperature is therefore to suppress ice-forming processes (and allow ice-depleting processes) within certain temperature ranges.

Note that we generally do not perturb processes involving the vapor phase, except for two exceptions described below. The rationale for this choice is that we

TABLE A1. Perturbed cloud microphysical processes in AM2.1. Processes are grouped based on the species they involve, and sorted by decreasing importance in terms of the mean, vertically integrated rate at 50° in the control experiment (column 5); missing rates are denoted by a dash. The variable name refers to the name of the output field. We omit all processes involving the vapor phase, which are not perturbed in our experiments. See text in Appendix A for details. A detailed description of the AM2.1 cloud microphysics is available under http://data1.gfdl.noaa.gov/~arl/pubrel/m/am2/src/atmos_param/strat_cloud/strat_cloud.tech.ps.

Type	Process name	Variable name	Temperature range (°C)	Mean vertically integrated rate at 50° ($kg\,m^{-2}\,day^{-1}$)
Liquid → ice	WBF	qldt_berg	$T < 0$	1.30
	Riming	qldt_rime	$T < 0$	0.89
	Homogeneous freezing	qldt_freez	$T < -40$	0.00
Ice → rain	Ice melting	qidt_melt	$T > 0$	0.17
Snow → rain	Snow melting	snow_melt	$T > 0$	—

wish to demonstrate the importance of the ice-phase processes that deplete cloud liquid water for the LWP response in mixed-phase regions, excluding contributions from changes in the sources of cloud condensate from vapor. The only exceptions to this rule are ice nucleation as well as WBF, both in CESM-CAM5 only. In the CESM-CAM5 implementation, the WBF process can form cloud ice at the expense of either liquid water or vapor, depending on the availability of cloud liquid water in the grid box (Gettelman et al. 2010). Ice nucleation is included as a microphysical process in CESM-CAM5, and depends on both temperature and the presence of activated ice nuclei (Gettelman et al. 2010). In AM2.1, homogeneous ice nucleation is implicitly treated in the large-scale condensation/deposition scheme rather than in the microphysics, and is therefore not included in our experiments; heterogeneous

nucleation is not represented. We have verified that perturbing homogeneous nucleation has a negligible effect on the cloud liquid water and ice response to warming in AM2.1 (not shown).

For most of the microphysical processes, the temperature perturbation only affects the temperature threshold that controls the occurrence of the process. For example, the 4-K temperature increase suppresses the WBF process in regions where the "real" temperature is between 0 and −4 K. In addition to the temperature thresholds that control the occurrence of ice-phase processes, however, a few of the process rates are also explicit functions of temperature. In CESM-CAM5 (Table A2), these are all types of heterogeneous freezing (MNUCCCO, MNUCCTO, MNUCCRO). In AM2.1, the WBF process rate is also linearly dependent on temperature; however, this linear function is an

TABLE A2. Perturbed cloud microphysical processes in CESM-CAM5. Symbols and definitions are as in Table A1. When available, the variable name refers to the output field (uppercase), or the internally stored variable in the code (lowercase). Missing values are denoted by a dash. For details on the CESM-CAM5 cloud microphysics, see Morrison and Gettelman (2008) and Gettelman et al. (2010).

Type	Process name	Variable name	Temperature range (°C)	Mean vertically integrated rate at 50° ($kg\,m^{-2}\,day^{-1}$)
Vapor → ice	Homogeneous + heterogeneous ice nucleation	MNUCCDO	$T < -5$	0.00
Liquid → ice	WBF	BERGO	$T < 0$	0.31
	Immersion freezing	MNUCCCO	$T < -4$	0.00
	Contact freezing	MNUCCTO	$T < -3$	0.00
	Homogeneous freezing	HOMOO	$T < -40$	0.00
	Rime-splintering	MSACWIO	$-8 < T < -3$	0.00
Ice → liquid	Melting	MELTO	$T > 0$	0.00
Liquid → snow	WBF on snow	BERGSO	$T < 0$	0.26
	Accretion by snow	PSACWSO	$T < 0$	0.25
Ice → snow	Autoconversion	PRCIO	$T < 0$	1.36
	Accretion by snow	PRAIO	$T < 0$	0.05
Rain → snow	Accretion by snow	PRACSO	$T < 0$	0.68
	Heterogeneous freezing of rain	MNUCCRO	$T < -4$	0.28
	Homogeneous freezing of rain	—	$T < -5$	—
Snow → rain	Snow melting	—	$T > +2$	—
Snow → snow	Snow self-aggregation	nsagg	$T < 0$	—

approximation to the dependence of saturation vapor pressure terms on temperature, as described above, so that perturbing temperature is equivalent to perturbing vapor pressures in the WBF process in CESM-CAM5.

In addition to the processes listed in Tables A1 and A2, the microphysics schemes include a temperature-dependent removal of excess supersaturation (also called adjustment in the AM2.1 code). Supersaturation may occur at the end of the microphysics scheme due to nonlinearity and numerical errors in calculating water vapor tendencies. Forced condensation/deposition is therefore applied to remove the excess water vapor, and the partitioning of the resulting condensate between liquid water and ice is the same as that used for the partitioning of detrained convective condensate in each of the models (see section 3a). While the temperature partitioning of the removal of excess supersaturation is not perturbed in our experiments, we have verified that the results are not sensitive to the inclusion of this process (not shown).

APPENDIX B

List of CMIP5 Models and Variables Used in the Paper

Table B1 lists the models and fields used in our analysis and shown in Figs. 1 and 8 of the paper. For all models, we use monthly mean values and the first ensemble member only (r1i1p1).

For reference, below we also describe the CMIP5 variables used in the analysis. For liquid and ice water paths, we use the variables clwvi (total condensed water path) and clivi (IWP), with LWP calculated as the difference between clwvi and clivi. Note that for several models, clwvi erroneously reports only LWP, instead of the sum of LWP and IWP, as described in the CMIP5 errata available under http://cmip-pcmdi.llnl.gov/cmip5/errata/cmip5errata.html. For those models, this results in negative LWP values when calculated as clwvi minus clivi. We identify those models based on the absolute minimum value of clwvi minus clivi, using a threshold of $-1 \, g \, m^{-2}$ for any grid point and month. (We use -1 rather than $0 \, g \, m^{-2}$ because several models have weakly negative minimum values for both LWP and IWP.) The models for which clwvi erroneously represents LWP based on our criterion are marked with an asterisk in Table B1.

The SW radiation fields mentioned in Table B1 include all variables required for the approximate partial radiative perturbation (APRP) calculation presented in Fig. 1a: these include rsdt, rsut, rsutcs, rsds, rsdscs, rsus,

TABLE B1. List of CMIP5 models used in Figs. 1 and 8. The historical and RCP8.5 periods are 1980–99 and 2080–99, respectively. A cross (×) indicates that the data were available at the time of writing. Models marked with an asterisk (*) reported condensed water path variables erroneously, as described in appendix B. The models included in the second column are used in Fig. 8, while those in the third column are used in Fig. 1.

	Model name	LWP, IWP, and temperature	SW radiation fields
1	ACCESS1.0	×	×
2	ACCESS1.3	×	×
3	BCC-CSM1.1	×	×
4	BCC-CSM1.1(m)	×	×
5	CanESM2	×	×
6	*CCSM4	×	×
7	*CESM1-BGC	×	×
8	*CESM1-CAM5	×	×
9	*CMCC-CESM	×	
10	*CMCC-CM	×	
11	CNRM-CM5	×	×
12	CSIRO-Mk3.6.0	×	×
13	FGOALS-g2	×	
14	FIO-ESM	×	×
15	GFDL-CM3	×	×
16	GFDL-ESM2G	×	×
17	GFDL-ESM2M	×	×
18	GISS-E2-H	×	×
19	GISS-E2-R	×	×
20	HadGEM2-CC	×	×
21	INM-CM4	×	×
22	*IPSL-CM5A-LR	×	×
23	*IPSL-CM5A-MR	×	×
24	*IPSL-CM5B-LR	×	×
25	MIROC5	×	×
26	*MIROC-ESM	×	×
27	*MIROC-ESM-CHEM	×	×
28	*MPI-ESM-LR	×	×
29	*MPI-ESM-MR	×	×
30	MRI-CGCM3	×	×
31	NorESM1-M	×	×
32	NorESM1-ME	×	×

rsuscs, and clt. Finally, for surface and lower-tropospheric temperature we use ts and ta, respectively.

REFERENCES

Anderson, J. L., and Coauthors, 2004: The new GFDL global atmosphere and land model AM2LM2: Evaluation with prescribed SST simulations. *J. Climate*, **17**, 4641–4673, doi:10.1175/JCLI-3223.1.

Barnes, E. A., and L. Polvani, 2013: Response of the midlatitude jets and of their variability to increased greenhouse gases in the CMIP5 models. *J. Climate*, **26**, 7117–7135, doi:10.1175/JCLI-D-12-00536.1.

Bender, F. A.-M., V. Ramanathan, and G. Tselioudis, 2012: Changes in extratropical storm track cloudiness 1983–2008: Observational support for a poleward shift. *Climate Dyn.*, **38**, 2037–2053, doi:10.1007/s00382-011-1065-6.

Bergeron, T., 1935: On the physics of clouds and precipitation. *Procès-Verbaux de l'Association de Météorologie*, International Union of Geodesy and Geophysics, 156–178.

Betts, A. K., and Harshvardhan, 1987: Thermodynamic constraint on the cloud liquid water feedback in climate models. *J. Geophys. Res.*, **92**, 8483–8485, doi:10.1029/JD092iD07p08483.

Boucher, O., and Coauthors, 2013: Clouds and aerosols. *Climate Change 2013: The Physical Science Basis*, T. F. Stocker et al., Eds., Cambridge University Press, 571–657.

Ceppi, P., and D. L. Hartmann, 2015: Connections between clouds, radiation, and midlatitude dynamics: A review. *Curr. Climate Change Rep.*, **1**, 94–102, doi:10.1007/s40641-015-0010-x.

——, Y.-T. Hwang, D. M. W. Frierson, and D. L. Hartmann, 2012: Southern Hemisphere jet latitude biases in CMIP5 models linked to shortwave cloud forcing. *Geophys. Res. Lett.*, **39**, L19708, doi:10.1029/2012GL053115.

——, M. D. Zelinka, and D. L. Hartmann, 2014: The response of the Southern Hemispheric eddy-driven jet to future changes in shortwave radiation in CMIP5. *Geophys. Res. Lett.*, **41**, 3244–3250, doi:10.1002/2014GL060043.

Cesana, G., D. E. Waliser, X. Jiang, and J.-L. F. Li, 2015: Multi-model evaluation of cloud phase transition using satellite and reanalysis data. *J. Geophys. Res. Atmos.*, **120**, 7871–7892, doi:10.1002/2014JD022932.

Choi, Y.-S., C.-H. Ho, C.-E. Park, T. Storelvmo, and I. Tan, 2014: Influence of cloud phase composition on climate feedbacks. *J. Geophys. Res. Atmos.*, **119**, 3687–3700, doi:10.1002/2013JD020582.

Colman, R., J. Fraser, and L. Rotstayn, 2001: Climate feedbacks in a general circulation model incorporating prognostic clouds. *Climate Dyn.*, **18**, 103–122, doi:10.1007/s003820100162.

Dee, D. P., and Coauthors, 2011: The ERA-Interim reanalysis: Configuration and performance of the data assimilation system. *Quart. J. Roy. Meteor. Soc.*, **137**, 553–597, doi:10.1002/qj.828.

Feigelson, E. M., 1978: Preliminary radiation model of a cloudy atmosphere. Part I: Structure of clouds and solar radiation. *Beitr. Phys. Atmos.*, **51**, 203–229.

Findeisen, W., 1938: Die kolloidmeteorologischen Vorgänge bei Niederschlagsbildung. *Meteor. Z.*, **55**, 121–133.

Gettelman, A., and Coauthors, 2010: Global simulations of ice nucleation and ice supersaturation with an improved cloud scheme in the Community Atmosphere Model. *J. Geophys. Res.*, **115**, D18216, doi:10.1029/2009JD013797.

Gordon, N. D., and S. A. Klein, 2014: Low-cloud optical depth feedback in climate models. *J. Geophys. Res. Atmos.*, **119**, 6052–6065, doi:10.1002/2013JD021052.

Grise, K. M., and L. M. Polvani, 2014: Southern Hemisphere cloud-dynamics biases in CMIP5 models and their implications for climate projections. *J. Climate*, **27**, 6074–6092, doi:10.1175/JCLI-D-14-00113.1.

——, ——, G. Tselioudis, Y. Wu, and M. D. Zelinka, 2013: The ozone hole indirect effect: Cloud-radiative anomalies accompanying the poleward shift of the eddy-driven jet in the Southern Hemisphere. *Geophys. Res. Lett.*, **40**, 3688–3692, doi:10.1002/grl.50675.

Gultepe, I., and G. A. Isaac, 1997: Liquid water content and temperature relationship from aircraft observations and its applicability to GCMs. *J. Climate*, **10**, 446–452, doi:10.1175/1520-0442(1997)010<0446:LWCATR>2.0.CO;2.

Held, I. M., and B. J. Soden, 2006: Robust responses of the hydrological cycle to global warming. *J. Climate*, **19**, 5686–5699, doi:10.1175/JCLI3990.1.

Heymsfield, A. J., and Coauthors, 2008: Testing IWC retrieval methods using radar and ancillary measurements with in situ

data. *J. Appl. Meteor. Climatol.*, **47**, 135–163, doi:10.1175/2007JAMC1606.1.

Hurrell, J. W., and Coauthors, 2013: The Community Earth System Model: A framework for collaborative research. *Bull. Amer. Meteor. Soc.*, **94**, 1339–1360, doi:10.1175/BAMS-D-12-00121.1.

Hwang, Y.-T., and D. M. W. Frierson, 2013: Link between the double–intertropical convergence zone problem and cloud biases over the Southern Ocean. *Proc. Natl. Acad. Sci. USA*, **110**, 4935–4940, doi:10.1073/pnas.1213302110.

Kay, J. E., B. Medeiros, Y.-T. Hwang, A. Gettelman, J. Perket, and M. G. Flanner, 2014: Processes controlling Southern Ocean shortwave climate feedbacks in CESM. *Geophys. Res. Lett.*, **41**, 616–622, doi:10.1002/2013GL058315.

Klein, S. A., and Coauthors, 2009: Intercomparison of model simulations of mixed-phase clouds observed during the ARM Mixed-Phase Arctic Cloud Experiment. I: Single-layer cloud. *Quart. J. Roy. Meteor. Soc.*, **135**, 979–1002, doi:10.1002/qj.416.

Kodama, C., S. Iga, and M. Satoh, 2014: Impact of the sea surface temperature rise on storm-track clouds in global non-hydrostatic aqua planet simulations. *Geophys. Res. Lett.*, **41**, 3545–3552, doi:10.1002/2014GL059972.

Komurcu, M., and Coauthors, 2014: Intercomparison of the cloud water phase among global climate models. *J. Geophys. Res. Atmos.*, **119**, 3372–3400, doi:10.1002/2013JD021119.

McCoy, D. T., D. L. Hartmann, and D. P. Grosvenor, 2014a: Observed Southern Ocean cloud properties and shortwave reflection. Part I: Calculation of SW flux from observed cloud properties. *J. Climate*, **27**, 8836–8857, doi:10.1175/JCLI-D-14-00287.1.

——, ——, and ——, 2014b: Observed Southern Ocean cloud properties and shortwave reflection. Part II: Phase changes and low cloud feedback. *J. Climate*, **27**, 8858–8868, doi:10.1175/JCLI-D-14-00288.1.

——, ——, M. D. Zelinka, P. Ceppi, and D. P. Grosvenor, 2015: Mixed-phase cloud physics and Southern Ocean cloud feedback in climate models. *J. Geophys. Res. Atmos.*, **120**, 9539–9554, doi:10.1002/2015JD023603.

Morrison, H., and A. Gettelman, 2008: A new two-moment bulk stratiform cloud microphysics scheme in the Community Atmosphere Model, version 3 (CAM3). Part I: Description and numerical tests. *J. Climate*, **21**, 3642–3659, doi:10.1175/2008JCLI2105.1.

Neale, R. B., and B. J. Hoskins, 2000: A standard test for AGCMs including their physical parametrizations: I: The proposal. *Atmos. Sci. Lett.*, **1**, 101–107, doi:10.1006/asle.2000.0022.

——, and Coauthors, 2012: Description of the NCAR Community Atmosphere Model (CAM 5.0). NCAR Tech. Note NCAR/TN-485+STR, 212 pp.

O'Dell, C. W., F. J. Wentz, and R. Bennartz, 2008: Cloud liquid water path from satellite-based passive microwave observations: A new climatology over the global oceans. *J. Climate*, **21**, 1721–1739, doi:10.1175/2007JCLI1958.1.

Rotstayn, L. D., 1997: A physically based scheme for the treatment of stratiform clouds and precipitation in large-scale models. I: Description and evaluation of the microphysical processes. *Quart. J. Roy. Meteor. Soc.*, **123**, 1227–1282. doi:10.1002/qj.49712354106.

——, B. F. Ryan, and J. J. Katzfey, 2000: A scheme for calculation of the liquid fraction in mixed-phase stratiform clouds in large-scale models. *Mon. Wea. Rev.*, **128**, 1070–1088, doi:10.1175/1520-0493(2000)128<1070:ASFCOT>2.0.CO;2.

Senior, C. A., and J. F. B. Mitchell, 1993: Carbon dioxide and climate: The impact of cloud parameterization. *J. Climate*, **6**, 393–418, doi:10.1175/1520-0442(1993)006<0393:CDACTI>2.0.CO;2.

Sherwood, S. C., S. Bony, O. Boucher, C. Bretherton, P. M. Forster, J. M. Gregory, and B. Stevens, 2015: Adjustments in the

forcing-feedback framework for understanding climate change. *Bull. Amer. Meteor. Soc.*, **96**, 217–228, doi:10.1175/BAMS-D-13-00167.1.

Soden, B. J., and G. A. Vecchi, 2011: The vertical distribution of cloud feedback in coupled ocean–atmosphere models. *Geophys. Res. Lett.*, **38**, L12704, doi:10.1029/2011GL047632.

——, I. M. Held, R. Colman, K. M. Shell, J. T. Kiehl, and C. A. Shields, 2008: Quantifying climate feedbacks using radiative kernels. *J. Climate*, **21**, 3504–3520, doi:10.1175/2007JCLI2110.1.

Somerville, R. C. J., and L. A. Remer, 1984: Cloud optical thickness feedbacks in the CO_2 climate problem. *J. Geophys. Res.*, **89**, 9668–9672, doi:10.1029/JD089iD06p09668.

Stephens, G. L., 1978: Radiation profiles in extended water clouds. II: Parameterization schemes. *J. Atmos. Sci.*, **35**, 2123–2132, doi:10.1175/1520-0469(1978)035<2123:RPIEWC>2.0.CO;2.

Storelvmo, T., and I. Tan, 2015: The Wegener–Bergeron–Findeisen process—Its discovery and vital importance for weather and climate. *Meteor. Z.*, **24**, 455–461, doi:10.1127/metz/2015/0626.

Taylor, K. E., M. Crucifix, P. Braconnot, C. D. Hewitt, C. Doutriaux, A. J. Broccoli, J. F. B. Mitchell, and M. J. Webb, 2007: Estimating shortwave radiative forcing and response in climate models. *J. Climate*, **20**, 2530–2543, doi:10.1175/JCLI4143.1.

Tselioudis, G., W. B. Rossow, and D. Rind, 1992: Global patterns of cloud optical thickness variation with temperature. *J. Climate*, **5**, 1484–1495, doi:10.1175/1520-0442(1992)005<1484:GPOCOT>2.0.CO;2.

——, A. A. Lacis, D. Rind, and W. B. Rossow, 1993: Potential effects of cloud optical thickness on climate warming. *Nature*, **366**, 670–672, doi:10.1038/366670a0.

——, A. D. DelGenio, W. Kovari, and M.-S. Yao, 1998: Temperature dependence of low cloud optical thickness in the GISS GCM: Contributing mechanisms and climate implications. *J. Climate*, **11**, 3268–3281, doi:10.1175/1520-0442(1998)011<3268:TDOLCO>2.0.CO;2.

Tsushima, Y., and Coauthors, 2006: Importance of the mixed-phase cloud distribution in the control climate for assessing the response of clouds to carbon dioxide increase: a multi-model study. *Climate Dyn.*, **27**, 113–126, doi:10.1007/s00382-006-0127-7.

Vial, J., J.-L. Dufresne, and S. Bony, 2013: On the interpretation of inter-model spread in CMIP5 climate sensitivity estimates. *Climate Dyn.*, **41**, 3339–3362, doi:10.1007/s00382-013-1725-9.

Warren, S., C. Hahn, J. London, R. Chervin, and R. Jenne, 1988: Global distribution of total cloud cover and cloud type amounts over the ocean. NCAR Tech. Note TN-273+STR, 29 pp. + 200 maps.

Wegener, A., 1911: *Thermodynamik der Atmosphäre.* J. A. Barth (Leipzig), 331 pp.

Zelinka, M. D., S. A. Klein, and D. L. Hartmann, 2012: Computing and partitioning cloud feedbacks using cloud property histograms. Part II: Attribution to changes in cloud amount, altitude, and optical depth. *J. Climate*, **25**, 3736–3754, doi:10.1175/JCLI-D-11-00249.1.

——, ——, K. E. Taylor, T. Andrews, M. J. Webb, J. M. Gregory, and P. M. Forster, 2013: Contributions of different cloud types to feedbacks and rapid adjustments in CMIP5. *J. Climate*, **26**, 5007–5027, doi:10.1175/JCLI-D-12-00555.1.